JOURNAL OF THERMOPHYSICS AND HEAT TRANSFER
Vol. 20, No. 4, October–December 2006

Heat Transfer in Channels in Parallel-Mode Rotation at High Rotation Numbers

A. K. Sleiti* and J. S. Kapat†
University of Central Florida, Orlando, Florida 32816-2450

DOI: 10.2514/1.16634

This study attempts to understand one of the most fundamental and challenging problems in fluid flow and heat transfer for rotating machines. The study focuses on electric generators for high energy density applications, which employ rotating cooling channels so that materials do not fail under high temperature and high stress environment. Prediction of fluid flow and heat transfer inside internal cooling channels that rotate at high rotation number and high wall heat flux is the main focus of this study. Rotation, buoyancy, and boundary conditions affect the flow inside these channels. A fully computational approach is employed in this study. Reynolds stress turbulence model with enhanced near-wall treatment is validated against available experimental data (which are primarily at low rotation and buoyancy numbers). The model was then used for cases with high rotation number (as much as 0.35) and high wall heat flux. Particular attention is given to how turbulence intensity, Reynolds stresses, and transport are affected by Coriolis and buoyancy/centrifugal forces caused by high levels of rotation number and wall heat flux. Variations of flow total pressure along the rotating channel are also predicted. The results obtained are explained in view of physical interpretation of Coriolis and centrifugal forces.

Nomenclature

D_h	=	hydraulic diameter
DR	=	density ratio, $(T_w - T_o)/T_w$
f_{ce}	=	centrifugal force
f_{co}	=	Coriolis force
h	=	heat transfer coefficient
k	=	thermal conductivity of coolant
Nu	=	local Nusselt number, hD_h/K
Nu_o	=	Nusselt number in fully-developed turbulent nonrotating tube flow
Pr	=	Prandtl number
R	=	radius from axis of rotation
Re	=	Reynolds number, $W_o D_h/$
Ro	=	rotation number, $\Omega D_h/W_o$
S	=	distance in streamwise direction
T	=	local coolant temperature
T_o	=	coolant temperature at inlet
T_w	=	wall temperature
W_o	=	inlet velocity
$\Delta\rho/\rho$	=	density ratio, $(T_w - T_o)/T_w$, same as DR
θ	=	dimensionless temperature, $(T - T_o)/(T_w - T_o)$
μ	=	dynamic viscosity of coolant
ρ	=	density of air
Ω	=	rotational speed

Introduction

GENERATORS used for aircraft applications have high rotational speed compared with turbine-driven generators that in turn produce electrical power with a relatively high output per machine. The performance of these machines depends on stress, rotor vibrations, and thermal behavior. Once the physical size of the machine has been limited by the mechanical constraints, the only remaining way by which the power output may be increased is via increases in the electrical and magnetic loadings in the stator and rotor of the machine. The implied consequential increase in the absolute level of general inefficiencies within the machine necessitates a reliable cooling system to be incorporated into the fundamental design concept. This is to ensure that the thermal losses are dissipated at temperature levels compatible with an acceptable lifespan of the electrical insulation materials used in generator construction. Usually, the rotors of electrical machines are cooled by passing fluid inside hollow conductors that rotate parallel to the rotational axis (parallel-mode rotation). The shape of the coolant channels inside the windings of rotor can vary from square to circular. Figure 1 shows the windings of the rotor with their internal cooling channels, mounted in slots machined axially along the rotor forging. Figure 2 shows a schematic view of a square sectioned internal cooling channel, located inside copper winding of generator rotor. The Coriolis and centrifugal forces that are acting on the flowfield and the boundary conditions are shown.

Researchers have investigated heat transfer parameters using various types of coolants flowing in channels with Reynolds number ranging from 2000 to 37,000. Table 1 depicts a few assorted investigations along with the corresponding range of parameters (see Morris [1]). Morris provides theoretical, experimental, and numerical data for circular cross-section rotating channel for both laminar and turbulent flows. The available data in literature concerning rotating square channels is so limited. Morris also provides heat transfer measurements in square channels for low rotation number (in the range from 0.0125 to 0.063) and with maximum constant heat flux of 6.45 kW/m^2 for wall boundary condition.

Majumdar et al. [2] described theoretically some aspects of flow and heat transfer. Some agreement with measured Nusselt number was reported without providing precise details. The work by Dias [3] was extended by Morris and Dias [4] to include an experimental study of turbulent flow with air as a coolant. They found that for fixed Reynolds number, fixed eccentricity, and for a given constant heat flux, the heat transfer improved with increases in the rotational speed. They used the rotational Reynolds number, J_b, instead of the rotation number to express rotational effects. Their results showed that at each rotational speed, the local Nusselt number distributions had similar trends. Near the channel entrance, the initially high region of heat transfer asymptotes towards a plateau region consistent with

Presented as Paper 2554 at the Portland, Oregon Co-located Conferences, Portland, OR, 28 June–2 July 2004; received 15 March 2005; revision received 12 September 2005; accepted for publication 23 September 2005.

*Ph.D., research scholar/scientist and instructor, Department of Mechanical, Materials, and Aerospace Engineering, 4000 Central Florida Boulevard. Member AIAA.

†Professor of mechanical engineering, and Lockeed Martin Professor of engineering, Department of Mechanical, Materials, and Aerospace Engineering, 4000 Central Florida Boulevard. Associate Fellow AIAA.

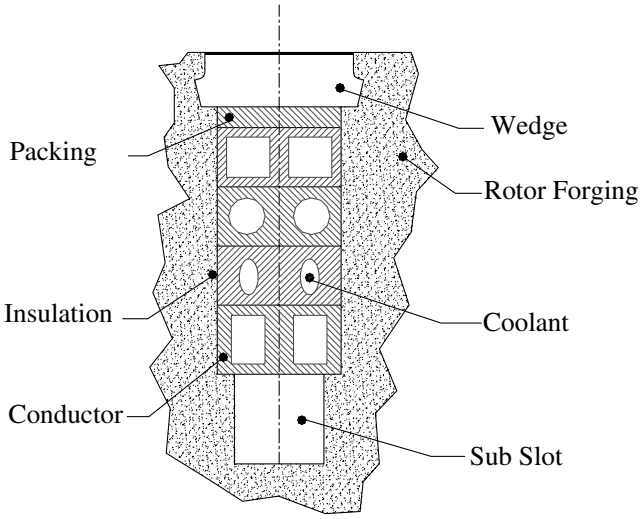

Fig. 1 Internal cooling channels geometries in copper winding of rotor slot.

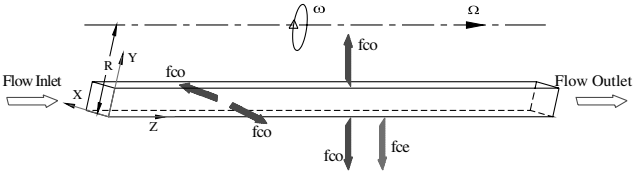

Fig. 2 Square sectioned internal cooling channel, located inside copper winding of generator rotor.

boundary layer development that occurs in a heated tube. Near the channel exit, the local heat transfer increases again due to the combination of the exit type effects and end conduction type. It was noted that there is a systematic improvement in the local heat transfer with increasing rotational speed for the rotational speed range studied. There was also a slight tendency for the Nusselt number to increase with increases in heat flux, which suggested that there was still a buoyancy effect even in turbulent flow regime. Morris and Dias also derived the following correlating equation for the mean Nusselt number:

$$Nu_m = 0.012Re^{0.78}J_b^{0.1} \tag{1}$$

where $J_b = \Omega b^2/2\mu$ and b is the duct height. Equation (1) correlates data with a maximum scatter of $+-14\%$ and was derived from data covering the range $120 < J_b < 620$, $32 < R/D_h < 48$, and $500 < Re < 20,000$ for $L/D_h = 48$. They compared the results using Eq. (1) with equation for circular channels derived by Morris and Woods [5] and with works of Humphreys (1966) and Le Feurre (1968) (see Morris). It has been noted that the results of Eq. (1) are in better agreement than the results using circular channels correlation. Thus the data from circular cross-section tubes is not recommended for square cross-sectioned channels.

Literature review reveals that most of these studies have concentrated on laminar Nusselt number and C_f (friction factor) for a range of rotational speeds from 300 rpm to a maximum of 2700 rpm. Generator rotors in practical applications can rotate at speeds as high as 90,000 rpm. The flowfield and heat transfer at such high speeds have different characteristics.

On the other hand, research with reference to internal cooling of gas turbines (orthogonal-mode rotation) is very intensive and has been addressed by many researchers, see Han et al. [6], Jang et al. [7], Rigby et al. [8], and Shih and Sultanian [9]. All these researchers have concentrated on low rotation number and low-density ratios cases. The authors in [10–12] investigated smooth-wall and rib-roughened channels using Reynolds stress model (RSM) turbulence models for the cases of high rotation number and high-density ratios cases.

One of the objectives of this research is to explore the flow phenomena and heat transfer in square sectioned channels rotating at high rotation number and high wall heat. This study examines the rich interplay of physics under the simultaneous actions of Coriolis and centrifugal/buoyancy forces in one of the most challenging internal flow configurations. Several important conclusions are reached from this computational study that may have far-reaching implications on how generator rotors are currently designed. Fluent computational fluid dynamics (CFD) code is used for this study.

Governing Equations

The continuity, momentum, and energy equations for a Newtonian compressible fluid are given as

$$\frac{\partial \rho}{\partial t} + \frac{\partial \rho U_i}{\partial x_i} = 0 \tag{2}$$

$$\frac{\partial \rho U_i}{\partial t} + \frac{\partial \rho U_i U_j}{\partial x_i} = \rho g_i + F_i - \frac{\partial P}{\partial x_i} + \frac{\partial}{\partial x_i}(2\mu S_{ij}) \tag{3}$$

$$\frac{\partial \rho E_0}{\partial t} + \frac{\partial \rho U_i E_0}{\partial x_i} = \rho U_i F_i - \frac{\partial q_i}{\partial x_i} + \frac{\partial}{\partial x_j}(U_i T_{ij}) \tag{4}$$

where F_i are the additional body-forces that can affect the fluid motion such as rotation, magnetic, or electric field, etc., s_{ij} is the strain rate tensor, T_{ij} are the surface forces similar to the viscous and pressure terms in the momentum equations, and E_0 is the total

Table 1 Experimental investigations on heat transfer and turbulence in parallel-mode rotating ducts

Authors	Topic	Duct cross-section	RP M	Re	Final outcome	L/D_h
Morris, D., 1964	HT laminar heated flow	Circular	300	10,000	Nu, C_f	24
Davies and Morris, D., 1965	HT laminar heated flow	Circular	300	10,000	Nu, C_f	24
Humphreys, 1966	Entrance turbulent	Circular	300	20,000	Nu, C_f	48
Humphreys and Morris, 1967	Entrance turbulent	Circular	300	20,000	Nu, C_f	6
Le Feurre, 1968	Entrance turbulent	Circular	300	20,000	Nu, C_f	2
Morris, D., 1968, 1970	HT laminar heated flow	Circular	300	10,000	Nu, C_f	24
Jakamota and Fukui, 1971	HT Laminar heated flow	Circular	2700	31,900	Nu, C_f	10
Woods and Morris, 1974	HT laminar heated flow	Circular	1500	2,500	Nu, C_f	24
Woods, 1975	HT laminar heated flow	Circular	1000	2,500	Nu, C_f	28
Skiadaressis and Spalding, 1976	Entrance laminar	Circular	1000	2,500	Nu, C_f	24
Morris and Woods, 1978	Entrance turbulent	Circular	1000	20,000	Nu, C_f	48
Nukayama and Fuzoika, 1978	Dev. turbulent	Circular	1000	37,000	Nu, C_f	27.3
Morris, 1980, 1981	Dev. laminar, isothermal, incompressible	Circular	600	10,000	Nu, C_f	24
Dias, 1978, and Morris and Dias, 1981	Exp. developed laminar HT, air	Square	300	2,000	Nu	51
Dias, 1978, and Morris and Dias, 1981	Exp. laminar HT in the entrance region, air	Square	300	2,000	Nu	32
Dias, 1978, and Morris and Dias, 1981	Exp. turbulent HT, air	Square	600	10,000	Nu	32

internal energy. Assuming constant rotation velocity the extra terms due to rotation are

$$a_i^{ce} = \varepsilon_{ijk}\varepsilon_{klm}\Omega_j\Omega_l x_m \qquad a_i^{co} = 2\varepsilon_{ijk}\Omega_j U_k \tag{5}$$

These terms are considered as body-force modification to Navier–Stokes equations and are added to the right-hand side of the momentum equation.

Computational Approach

Reynolds stress model [13–15] solves the Reynolds stresses, $\tau_{ij} = \overline{u_i' u_j'}$, using individual transport equations. The exact transport equations for the transport of the Reynolds stresses may be written as follows:

$$\frac{D\tau_{ij}}{Dt} = D_{T,ij} + D_{L,ij} + P_{ij} + G_{ij} + \phi_{ij} - \varepsilon_{ij} + F_{ij} + S \tag{6}$$

where $D\tau_{ij}/Dt = (\partial/\partial t)(\rho\overline{u_i' u_j'}) + C_{ij}$ and $(\partial/\partial t)(\rho\overline{u_i' u_j'})$ is the local time derivative, C_{ij} the convection term, $D_{T,ij}$ the turbulent diffusion term, $D_{L,ij}$ the molecular (viscous) diffusion term, P_{ij} the stress production term, G_{ij} the buoyancy production term, ϕ_{ij} the pressure-strain term, ε_{ij} the dissipation term, F_{ij} the production term by system rotation, and S the source term. Of the various terms in these exact equations, C_{ij}, $D_{L,ij}$, P_{ij}, and F_{ij} do not require any modeling. However, turbulent diffusion ($D_{T,ij}$), buoyancy production (G_{ij}), pressure-strain (ϕ_{ij}), and dissipation (ε_{ij}) need to be modeled to close the equations. These terms are given as

$$C_{ij} = \frac{\partial}{\partial x_k}(\rho u_k \overline{u_i' u_j'})$$

$$D_{T,ij} = -\frac{\partial}{\partial x_k}[\rho\overline{u_i' u_j' u_k'} + \overline{p(\delta_{kj}u_i' + \delta_{ik}u_j')}]$$

$$D_{L,ij} = \frac{\partial}{\partial x_k}\left[\mu\frac{\partial}{\partial x_k}(\overline{u_i' u_j'})\right] \qquad P_{ij} = -\rho\left(\overline{u_i' u_k'}\frac{\partial u_j}{\partial x_k} + \overline{u_j' u_k'}\frac{\partial u_i}{\partial x_k}\right)$$

$$G_{ij} = -\rho\beta(g_i\overline{u_j'\theta} + g_j\overline{u_i'\theta}) \qquad \phi_{ij} = \overline{p\left(\frac{\partial u_i'}{\partial x_j} + \frac{\partial u_j'}{\partial x_i}\right)}$$

$$F_{ij} = -2\rho\Omega_k(\overline{u_j' u_m'}\varepsilon_{ikm} + \overline{u_i' u_m'}\varepsilon_{jkm}) \qquad \varepsilon_{ij} = \frac{2}{3}\delta_{ij}(\rho\varepsilon + Y_M) \tag{7}$$

where $Y_M = 2\rho\varepsilon M_t^2$ is an additional dilatation dissipation. M_t is the turbulent Mach number defined as $M_t = \sqrt{(k/a^2)}$ where a is the speed of sound.

The pressure-strain term, ϕ_{ij}, is modeled according to the proposals by Gibson and Launder, Fu et al., and Launder (see [16]. Turbulent diffusive transport term, $D_{T,ij}$ is modeled by the generalized gradient-diffusion model of Daly and Harlow (see [16]. The Fluent manual [16] provides more details on modeling other terms.

Grid Generation and Boundary Conditions

Similar geometry to that studied by Morris [1] is chosen for the simulation. The channel is of square cross-section with length to hydraulic diameter ratio $L/D_h = 64$ and the eccentricity parameter $R/D_h = 32$; see Fig. 2. The inlet Reynolds number is fixed to 20,000 and uniform velocity profile is assumed at the inlet, whereas zero normal pressure gradient is set at the channel exit. To account for variations in fluid properties, the fluid density is calculated as for incompressible ideal gas, thermal conductivity and specific heat are calculated as functions of temperature, and viscosity is calculated using Sutherland formula. Rotation numbers considered are 0.0613, 0.14, and 0.3, which correspond to rotational Reynolds number J_b of 628, 1386, and 3472. Uniform wall heat flux boundary condition is applied for three cases of $q_1'' = 6450$ W/m^2, $q_2'' = 9000$ W/m^2 and $q_3'' = 12,000$ W/m^2. The highest rotational Reynolds number J_b and wall heat flux studied by Morris [1] were 628 and 6450 W/m^2, respectively. The experimental data given in Morris [1] were compared with results from this study for stationary ($Ro = 0$) and rotating ($Ro = 0.063$) cases. Two geometries are considered in this study; the first is with two side legs similar to the experimental geometry, where this geometry was used for comparison. The second geometry consists of one long channel without side legs, where the latest geometry is used for further investigations.

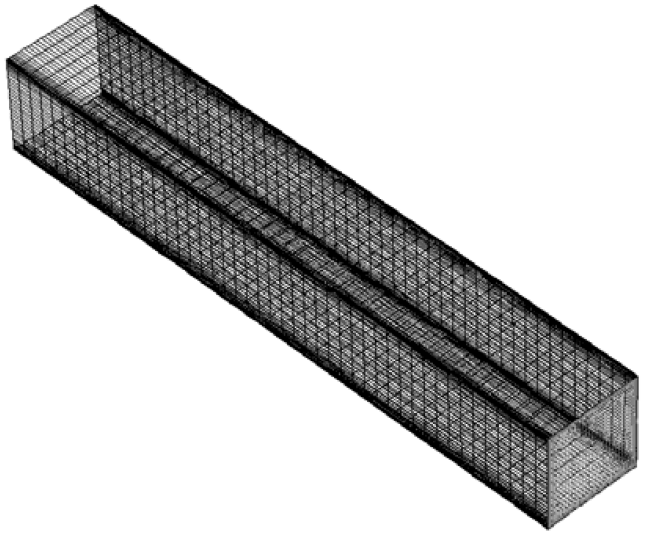

Fig. 3 Numerical grid for square channel in parallel-mode rotation.

Figure 3 gives the numerical grid generated using Gambit for this simulation. A grid refinement study is performed by investigating four numerical grids of $28 \times 28 \times 400$, $44 \times 44 \times 400$, $44 \times 44 \times 700$, and $62 \times 62 \times 1200$. Changing the grid distribution from $28 \times 28 \times 400$ to $44 \times 44 \times 400$ and $44 \times 44 \times 700$ showed a change in the Nusselt number of approximately 6 and 3%, respectively. Refining the grid further to $62 \times 62 \times 1200$ showed less than 0.8% change in the Nusselt number. Hence, the grid convergence is assumed reached with a grid of $44 \times 44 \times 700 = 1,355,200$ grid points, which is used for this simulation. Eleven grid points were placed near all walls, with y^+ of the cell next to a wall is less than one, to capture the flow and heat transfer details inside the boundary layer. The minimum convergence criteria for scaled residuals of pressure and all velocities were 10E-4 and 10E-9 for the energy equation.

Results

The influence of F_{ij} in Eq. (7) on the dynamics is investigated. With a rotation vector $\Omega^* = (0i + 0j + \Omega k)$, it follows from Eq. (7) that the Reynolds stresses equations contain additional terms as shown in Table 2.

The additional forces in parallel-mode rotation that are acting on the flow are

Coriolis force: $f_{co} = -2\rho(\Omega \times V)$, which in this case yields $f_{co} = 2\rho[i(\Omega v) - j(\Omega u)]$, which has two components. The first component acts toward the left surface (viewed from inlet in Fig. 2) when v is positive and toward right surface when v is negative. The second component acts toward bottom surface when u is positive and toward top surface when u is negative.

Centrifugal force: $f_{ce} = -\rho[\Omega \times (\Omega \times r)]$, which yields $f_{ce} = -j(\rho\Omega^2 r)$, which acts toward the bottom surface. Further discussion on the influence of F_{ij} in Eq. (7) on the dynamics is to be addressed in the following subsections.

Table 2 Influence of F_{ij} on dynamics in parallel-mode rotation

i, j	Reynolds stresses	F_{ij}	i, j	Reynolds stresses	F_{ij}
1, 1	$\overline{u'u'}$	$4\rho\Omega\overline{u'v'}$	1, 2	$\overline{u'v'}$	$2\rho\Omega\overline{u'u'} + 2\rho\Omega\overline{v'v'}$
2, 2	$\overline{v'v'}$	$-4\rho\Omega\overline{v'u'}$	1, 3	$\overline{v'v'}$	$2\rho\Omega\overline{(v'w')}$
3, 3	$\overline{w'w'}$	0	3, 2	$\overline{w'v'}$	$-2\rho\Omega\overline{(w'u')}$

Average and Local Nusselt Number

The heat transfer coefficient is calculated based on the fluid bulk temperature at each location reported. The bulk fluid temperature is defined as the mass weighted average temperature across the cross-section of interest. The fluid properties are calculated based on the local temperature of the fluid at locations of interest. The average Nusselt number values from this study were compared with experimental results of Morris [1] for $Ro = 0$ (no rotation) and $Ro = 0.063$ (the highest experimental rotation number) for wall heat flux of $q_1'' = 6450$ W/m^2. The comparison is shown in Fig. 4. The average Nusselt number from this study was taken as the average of the four sides of the channel, whereas in Morris [1] the local Nusselt number is provided and it is not clear whether the difference in Nusselt number between the four surfaces of the channel is considered. Moreover, the inlet and exit boundary conditions assumed in this study were different from the experimental boundary conditions, which are not known. Figure 4 shows that there is a maximum difference of up to 7% between measured and calculated Nusselt number. This difference is believed to be due to the difference in boundary conditions and may be due to differences between the experimental and predicted channel geometry. However, the difference of 7% is within experimental uncertainty.

The calculated local Nusselt number on the centerline of the leading surface of the channel is shown in Fig. 5. At the entrance of the channel the flow separates as the rotation number increases, which results in a Nusselt number increase up to $Z/L = 0.1$, then a sharp decrease up to $Z/L = 0.2$. After that the Nusselt number maintains a nearly constant value up to the exit of the duct. Increasing the rotation number causes an enhancement in heat transfer due to the effect of Coriolis force that acts toward leading surface, whereas increasing wall heat flux at high rotation number of 0.35 did not cause any further enhancement to the Nusselt nimber. On the centerline of the trailing surface (Fig. 6) almost the same behavior of the Nusselt number is observed as on the leading surface.

The highest values of the Nusselt number are found on the centerline of the bottom surface (Fig. 7), toward which the Coriolis and centrifugal forces are acting. Increasing Ro to 0.14 causes the Nusselt number to increase significantly, whereas further increase of Ro to 0.35 resulted in less increase in the Nusselt number beyond $Z/L = 0.5$. The explanation for this could be as follows: for $Ro = 0.14$, the effect of Coriolis force that acts toward the bottom surface adds to the effect of centrifugal force, which also acts toward the bottom surface, which increases the Nusselt number rapidly. By increasing Ro to 0.35, the centrifugal force increases, which in addition to Coriolis force effect enhances the Nusselt number, but at lower rate than for $Ro = 0.14$. Increasing wall heat flux at $Ro = 0.35$ decreases the Nusselt number slightly. On the centerline of the top surface (Fig. 8), the Nusselt number increases for $Z/L < 0.2$ as the rotation number and wall heat flux increase, then decreases rapidly for $Z/L > 0.2$. The strong centrifugal force pushes the colder fluid away from the top surface and thus the fluid near this surface is always hotter, which yields a lower Nusselt number.

These results of local Nusselt numbers on all four surfaces of the channel clearly show that due to effect of centrifugal and buoyancy forces the heat transfer rate differs substantially from each surface especially from top and bottom surfaces. The correlation for the Nusselt number given by Eq. (1). This suggests that new correlations as a function of rotation number and buoyancy parameter are needed to describe the heat transfer rate for each surface. This correlation should take into account both low and high rotation numbers and buoyancy parameter.

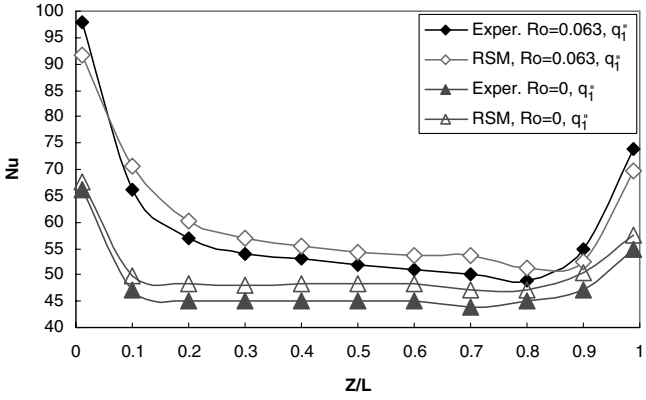

Fig. 4 Calculated average Nusselt number and measured local Nusselt number (Morris [1]).

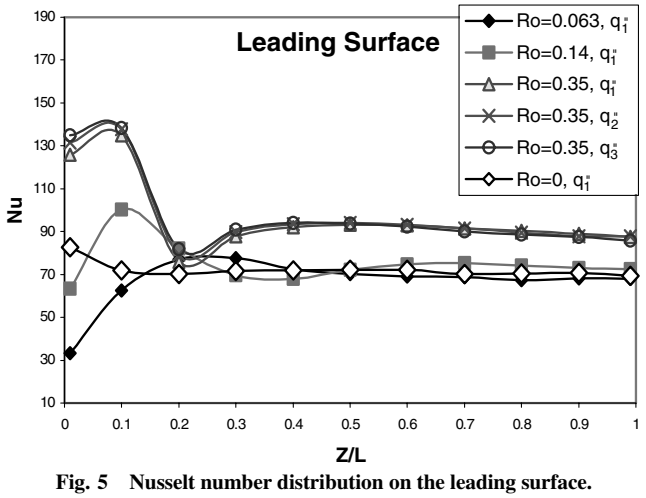

Fig. 5 Nusselt number distribution on the leading surface.

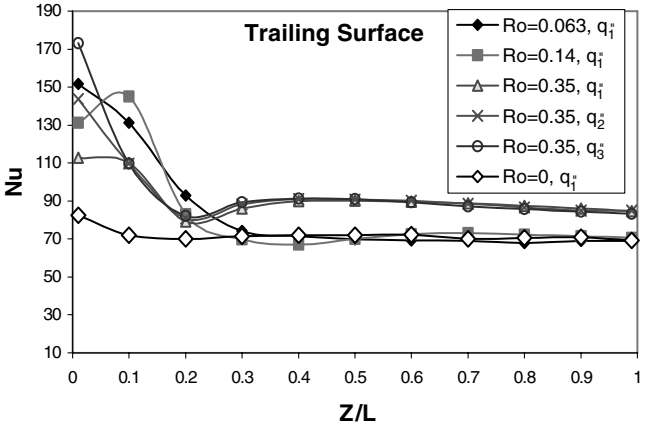

Fig. 6 Nusselt number distribution on the trailing surface.

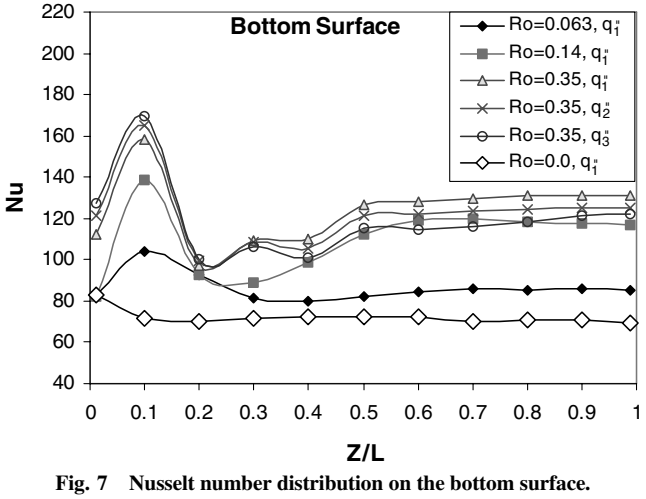

Fig. 7 Nusselt number distribution on the bottom surface.

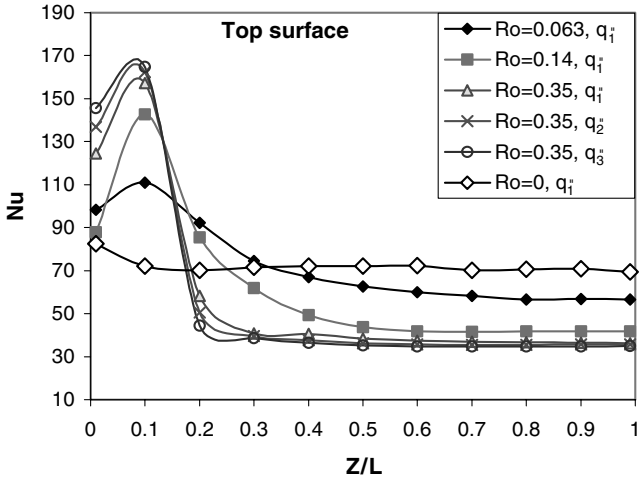

Fig. 8 Nusselt number distribution on the top surface.

Secondary Flow

The secondary flow vectors at three axial locations are shown in Fig. 9. At $Z/L = 0.3$, for low rotation numbers of 0.063 and 0.14, two vortices are formed near the leading-top and trailing-bottom surfaces. At this location for low rotation numbers, the combined effect of Coriolis and centrifugal forces caused the appearance of theses two vortices. Further downstream, the centrifugal force effect dominates, which resulted in two large vortices moving toward the bottom surface. The colder fluid is pushed toward the bottom surface, and then flows back near the leading and trailing surfaces, which caused an increase in the Nusselt number near theses surfaces.

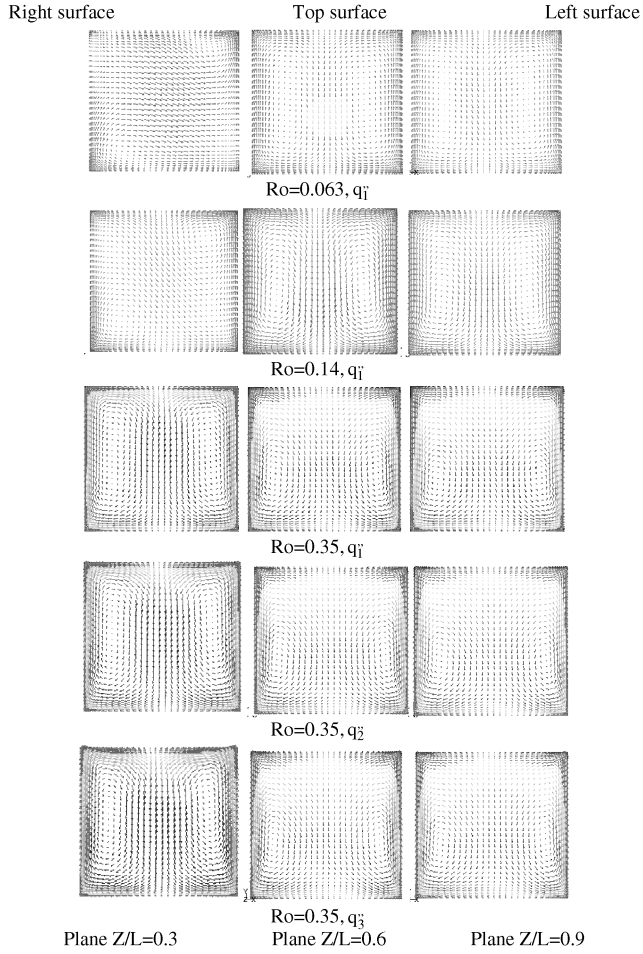

Fig. 9 Secondary flow vectors colored by streamwise velocity.

Increasing Ro to 0.35 increases the centrifugal force, which has more effect than the Coriolis force, resulting in two large vortices at $Z/L = 0.3$. The height of these vortices decreases downstream at locations $Z/L = 0.6$ and 0.9. Increasing wall heat flux at $Ro = 0.35$ did not change the structure of the vortices much.

Reynolds Shear Stress Components

Reynolds shear stress components are depicted in Fig. 10 at location $Z/L = 0.8$. According to Table 2, when $v'w'$ has the same sign as $w'u'$, then $w'u'$ acts as a sink to reduce $v'w'$, whereas when $v'w'$ has different sign than $w'u'$, then $w'u'$ acts as a source to add to $v'w'$. Both show that $w'u'$ always has the same sign as $v'w'$, hence $w'u'$ acts as a sink to reduce $v'w'$. As the rotation number and wall heat flux increase, $w'u'$ increases near both top and bottom surfaces, whereas $v'w'$ increases near bottom surface (yielding to increase the Nusselt number) and decreases with rotation (yielding to decrease the Nusselt number) then increases as wall heat flux increases near top surface. The increase of the $v'w'$ shear stress near the bottom surface enhances the heat transfer rate, whereas the decrease of $v'w'$ near the bottom surface decreases the heat transfer rate. As for the orthogonal-mode rotation, the slight increase in $v'w'$ due to increasing wall heat flux does not enhance heat transfer rate because the thermal boundary layer becomes thicker.

Reynolds Normal Stress Components and Turbulence Anisotropy

Figure 11 shows the normal stress components $w'w'$ and $v'v'$ at $Z/L = 0.8$. Normal stresses increase near bottom surface as the rotation number and wall heat flux increase and decrease near top surface as the rotation number increases, and then increase as wall heat flux increase. At $Ro = 0.063$ the flow is isotropic in the center of the channel. Increasing Ro to 0.14 and 0.35 the flow becomes

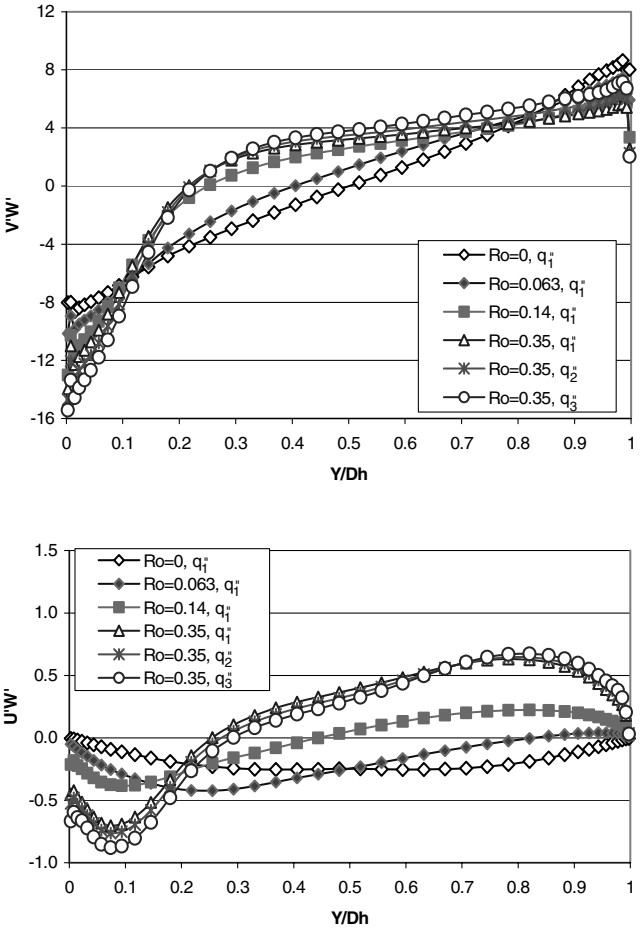

Fig. 10 Reynolds shear stress components (m^2/s^2) at $Z/L = 0.8$ and $X/D_h = 0.5$ ($Y/D_h = 0$ corresponds to bottom surface and $Y/D_h = 1$ corresponds to top surface).

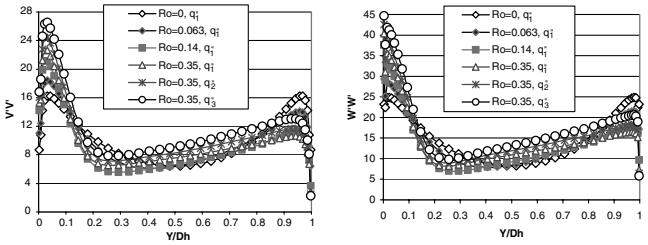

Fig. 11 Reynolds normal stress components (m^2/s^2) at $Z/L = 0.8$ and $X/D_h = 0.5$ ($Y/D_h = 0$ corresponds to bottom surface and $Y/D_h = 1$ corresponds to top surface).

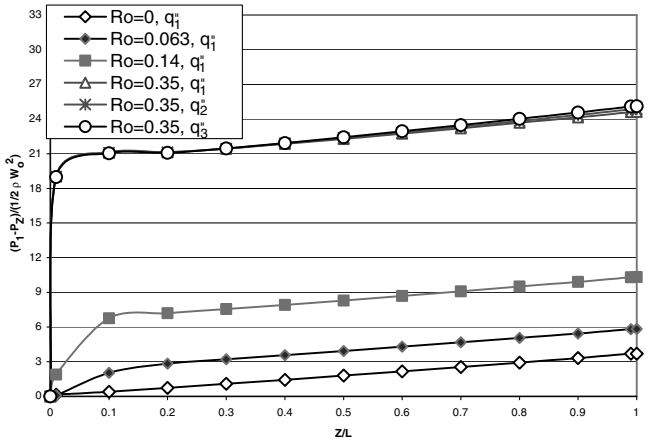

Fig. 12 Mass weighted average total pressure drop: parallel-mode rotation.

anisotropic. Increasing wall heat flux to $q''2$ reduced $w'w'/v'v'$, whereas further increase of wall heat flux to q''_3 increases $w'w'/v'v'$ slightly. Rotation has no effect on $w'w'$ (see Table 2), and thus the key component here is $v'v'$.

Mass Weighted Average Total Pressure Drop

The mass weighted average total pressure drop along the channel is calculated relative to inlet location (P_1). The results are shown in Fig. 12. The total pressure drop is increasing almost linearly with increasing rotation number because of the increasing effects of secondary flows, mixing, and friction.

Conclusions

Studying square internal cooling channels in parallel-mode rotation, the following is concluded: Increasing the rotation number enhances the heat transfer on three surfaces of the square channel and decreases the Nusselt number in the fourth surface. The average Nusselt number increases with increasing rotation number. This work demonstrates the need for Nusselt number correlations for each surface of the internal cooling channel, not just an overall average.

Increasing wall heat flux at high rotation numbers does not necessarily increase the Nusselt number on walls although higher turbulence activity is observed.

References

[1] Morris, W. D., *Heat Transfer and Fluid Flow in Rotating Coolant Channels:*, Research Studies, London, 1981.
[2] Majumdar, A. K., Morris, W. D., Skiadaressis, D., and Spalding, D. B., "Heat Transfer in Rotating Ducts," *Mechanical Engineering Bulletin*, Vol. 8, No. 4, 1977, p. 87.
[3] Dias, F. M., *Heat Transfer and Resistance to Flow in Rotating Square Tubes*, Univ. of Sussex, Falmer, England, 1978.
[4] Morris, W. D., and Dias, F. M., "Laminar Heat Transfer in Square Sectioned Ducts Which Rotate in the Parallel-Mode," *Power Industry Research*, Vol. 1, No. 1, 1981, pp. 1–29.
[5] Morris, W. D., and Woods, J. L., "Heat Transfer in the Entrance Region of Tubes that Rotate About a Parallel Axis," *Journal of Mechanical Engineering Science*, Vol. 20, June 1978, p. 319.
[6] Han, J. C., Dutta, S., and Srinath, E., *Gas Turbine Heat Transfer and Cooling Technology*, Taylor & Francis, New York, 2000.
[7] Jang, Y.-J., Chen, H.-C., and Han, J.-C., "Flow and Heat Transfer in a Rotating Square Channel with 45 deg Angled Ribs by Reynolds Stress Turbulence Model," *Journal of Turbomachinery*, Vol. 123, No. 2, 2001, pp. 124–132.
[8] Rigby, D. L., Steinthorsson, E., and Ameri, A., "Numerical Prediction of Heat Transfer in a Channel With Ribs and Bleed," ASME Paper No. 97-GT-431, 1997.
[9] Shih, T. I.-P., and Sultanian, B., *Computations of Internal and Film Cooling*, WIT, Ashurst, Southhampton, 2001.
[10] Sleiti, A. K., and Kapat, J. S., "Effect of Coriolis and Centrifugal Forces at High Rotation and Density Ratios," *Journal of Thermophysics and Heat Transfer*, Vol. 20, No. 1, 2006, pp. 67–79.
[11] Sleiti, A. K., and Kapat, J. S., "Fluid Flow and Heat Transfer in Rotating Curved Duct at High Rotation and Density Ratios," *Journal of Turbomachinery*, Vol. 127, No. 4, 2005, pp. 659–667.
[12] Sleiti, A. K., and Kapat, J. S., "Effect of Coriolis and Centrifugal Forces on Turbulence and Heat Transfer at High Rotation and Buoyancy Numbers in Rib-Roughened Internal Cooling Channel," American Society of Mechanical Engineers (ASME) Paper GT2004-53018, 2004.
[13] Gibson, M. M., and Launder, B. E., "Ground Effects on Pressure Fluctuations in the Atmospheric Boundary Layer," *Journal of Fluid Mechanics*, Vol. 86, No. 1, 1978, pp. 491–511.
[14] Launder, B. E., "Second-Moment Closure: Present...and Future?," *International Journal of Heat and Fluid Flow*, Vol. 10, No. 1, 1989, pp. 282–300.
[15] Launder, B. E., Reece, G. J., and Rodi, W., "Progress in the Development of a Reynolds-Stress Turbulence Closure," *Journal of Fluid Mechanics*, Vol. 68, No. 1, 1975, pp. 537–566.
[16] The FLUENT User's Guide, Ver. 6.2, FLUENT, Inc., New Hampshire.